Supplemental material: Behaviour of flexible superhydrophobic striped surfaces during (electro-)wetting of a sessile drop

Arvind Arun Dev[a,c], Ranabir Dey[b,c], Frieder Mugele[c]
[a] Department of magnetism of nanostructured objects (DMONS),
Institut de Physique et Chimie des Matèriaux de Strasbourg (IPCMS),
CNRS UMR 7504, Universitè de Strasbourg,
23 Rue du Loess, 67034 Strasbourg, France.
[b] Dynamics of Complex Fluids,
Max Planck Institute for Dynamics and Self-organization,
Am Fassberg 17, 37077 Goettingen, Germany.
[c] Physics of Complex Fluids, MESA+ Institute for Nanotechnology,
University of Twente, PO Box 217, 7500 AE
Enschede, The Netherlands

S1. Fabrication of soft striped superhydrophobic surface

The soft striped superhydrophobic surfaces are fabricated using a three step soft molding process. In the first step, we make a replica (primary) of our desired substrate using photolithography. In this step we get SU8 structured surface on a silicon wafer (see step 1 in Fig. S1). In the second step, we prepare a PDMS mold of the SU8 replica using Sylgard^{TM} 184, silicon elastomer. A mixture of base and cross-linker in 10:1 ratio by weight is mixed to prepare PDMS. This mixture is then poured on the primary SU8 obtained in step 1 and cured in vacuum at 60°C for 14 hrs. The PDMS mold is obtained by peeling off the cured PDMS from the SU8 primary; the PDMS mold essentially contains the negative imprint of the SU8 replica, i.e it contains empty slots corresponding to the lamellae (see step 2 in Fig. S1). This secondary PDMS mold is further cleaned using air plasma for 45 sec at 60W power and silanized with trichloro (1H,1H,2H,2H-perfluoro-octyl) silane from Sigma-Aldrich using chemical vapour deposition. In the third step, crosslinker of PDMS is mixed with fluorescent dye called DFSB-K175 from Risk Reactor in a ratio 1 ml to 3 μl. After thorough mixing, the base of elastomer kit is mixed with this solution in the desired ratio to get PDMS of different Young's modulus of elasticity (E). For the present work, we have used three different base to crosslinker ratios- 10:1, 15:1, 20:1 resulting in decreasing values of E (see Fig. S4; for details of the measurement of E see Sec. S2). Thereafter an ITO coated coverslip of thickness 175 μm is spin coated with PDMS+dye solution using a spin coater. The speed and acceleration parameters of spin coater used are 1000 rpm and 4000 rpm/s respectively. These spin coat parameters give the base thickness of the PDMS layer as 32 μm, 70 μm, and 100 μm for 10:1, 15:1 and 20:1 PDMS respectively. The coverslip with PDMS layer is then placed on the secondary PDMS mold which allows the

solution to fill the secondary mold and is then cured for 14 hrs at 60°C. Peeling off the PDMS mold from the coverslip gives the final sample which is soft striped superhydrophobic surface on a conductive coverslip (see Fig. S1).

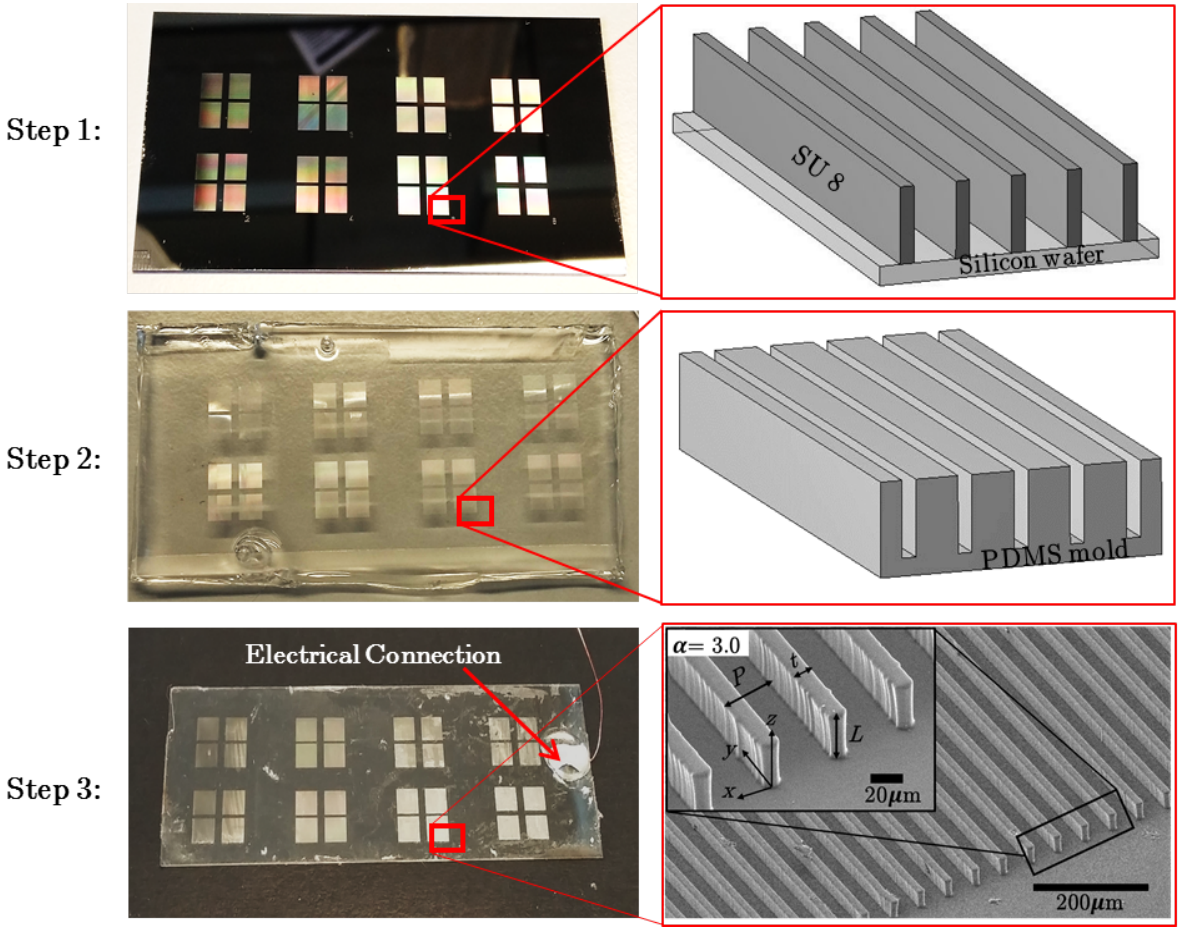

Figure S1: Fabrication process. Step 1: We get SU8 structures (shining squares) on silicon wafer (black base), magnified region shows the schematic of structures. Step 2: We get PDMS mold with empty spaces corresponding to SU8 structures, magnified image shows the empty slots in the soft mold. Step 3: We get soft structured surface on cover slip, magnified image shows the SEM image of sample. L denotes height of structure , t is thickness, w is width of structure in y direction and P is one pitch length of the structured surface. α denotes the aspect ratio (ratio of height to width) of the structure.

Step 3 (left) in Fig. S1 shows sample with electrical connection. The electrical connection on sample is made after scratching small part of PDMS from the coverslip. This scratch exposes the ITO coated conductive coverslip and copper wires are connected to this area. Step 3 (right) show SEM image of the soft structured surface. Inset in step 3 (right) shows a magnified region of the surface. The coordinate axes shown in the inset is followed throughout the article. x axis is across the lamellae, y axis is along the lamellae, and z axis corresponds with the height of the lamellae. Lamellae are continuous along y axis for w=3000 μm, whereas along x axis, the lamellae, each of thickness t, are separated by 37 μm (see Fig. S1).

S2. Measurement of Young's Modulus

Young's modulus of PDMS prepared with base to crosslinker ratio of 10:1, 15:1 and 20:1 is measured using extensometer from Zwick Roell. Fig. S2 shows the sample and setup for tensile testing. The test sample shown in Fig. S2(a) has a dumbbell shape. The wider portion is

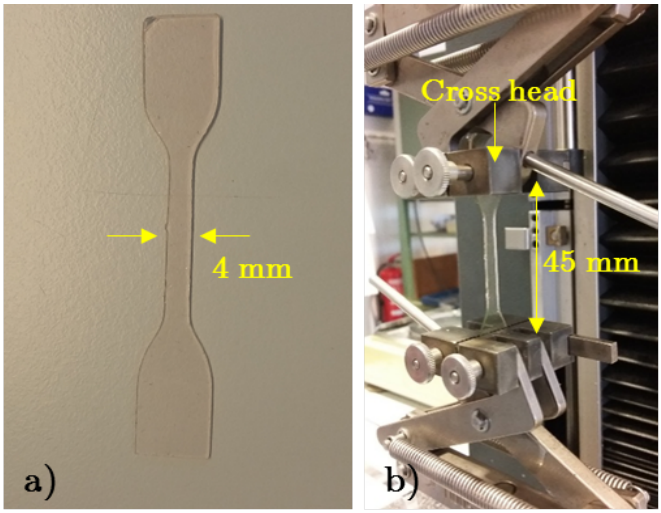

Figure S2: Tensile test. a) Sample of dumbbell shape with width =4mm, b) sample held in tensile machine.

gripped between the extensometer. The sample width is 4 mm and thickness 1 mm. Fig. S2(b) shows the sample gripped between the extensometer. The guage length of sample is 45 mm and the cross head velocity is 250 mm/s [1]. As the cross head moves with the specified velocity, the sample streches and the stress strain curve is obtained. Fig. S3 shows the stress-strain curve for PDMS with base to crosslinker ratios as 20:1 , 15:1 and 10:1. The strain in the test

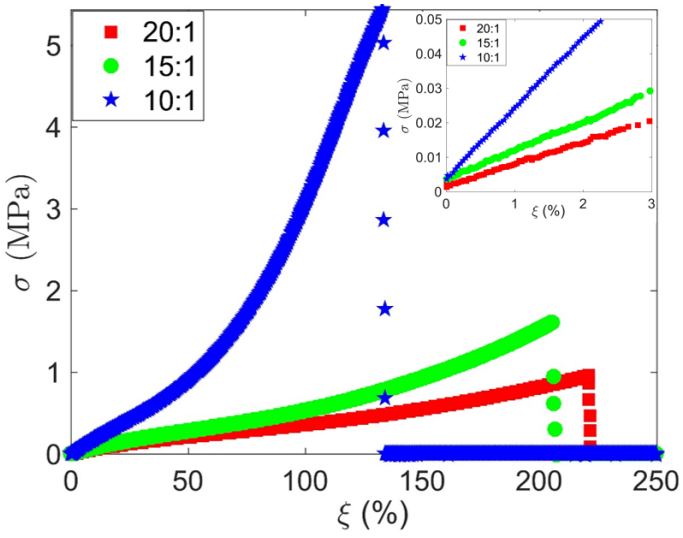

Figure S3: Stress-Strain curve for PDMS. ζ denotes strain in percentage and σ denotes the stress on the cross section of specimen. Inset shows the stress strain curve from 0 to 3% of strain where the the stress-strain curve is linear. Three different mixtures of PDMS as 20:1 ,15:1, 10:1 are measured.

sample increases with increasing stress. Inset in Fig. S3 shows that for the initial strain, the stress-strain curve is linear. In the linear region, the Young's modulus can be calculated by Hooke's law which defines Young's modulus as the slope of stress strain curve. The Young's modulus is calculated using the stress strain curve from 1% to 2% of the strain. For each cross linker to base ratio of PDMS, five measurements are done. Fig. S4 shows the experimentally calculated Young's modulus.

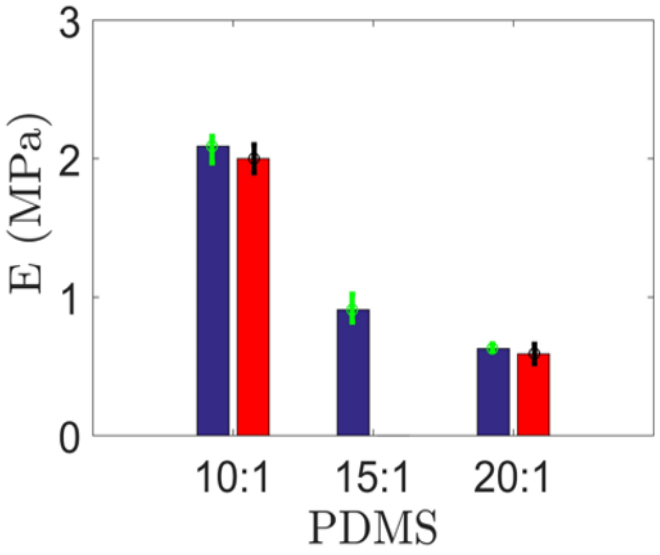

Figure S4: Young's modulus of PDMS. Blue bars are our experimental values and red bars are from literature [2] [3]. We could not find in literature the experimental value for 15:1, but 16.7 :1 mixture suggest 1.2 MPa [4]

The Young's modulus (E) of PDMS shown in figure is an average of 5 measurements. The value of E for base to crosslinker ratio 10:1, 15:1, and 20:1 PDMS is 2.1 MPa , 0.9 MPa and 0.6 MPa respectively. The Young's modulus of PDMS decreases with increase in the base content.

S3. Characterization of dyes for confocal microscopy

Fluorescent dyes are mixed in PDMS and in the drop. The dye used in PDMS is DFSB-K175 from Risk Reactor and the dye used in the drop is Wheat Germ Agglutinin, Alexa Fluor 647 Conjugate from ThermoFisher SCIENTIFIC. DFSB-K175 is mixed with the crosslinker of Sylgard elastomer kit in volume ratio of 1:3000. The Alexa 647 is mixed with water in the concentration of 5 μg/ml. This is stock solution and stored at 4°C. The drops used in experiments are mixture of the stock solution and 1mM KCl solution in a ratio of 1/100 by volume. The excitation and emission spectra of Alexa is available from chroma spectra viewer [5] while the excitation and emission spectra of DFSB-K175 is determined using spectrofluorometer. Fig. S5 shows the excitation and emission spectra for DFSB-K175 and Alexa 647.

The excitation and emission intensities in Fig. S5 are normalised by their maximum values for respective dyes. The excitation spectra of DFSB-K175 shown in Fig. S5(a) has two peaks, one at 494 nm and other at 530 nm. The emission spectra of DFSB-K175 is for 488 nm excitation and has emission maximum at 540 nm. Excitation and emission spectra of Alexa 647 in Fig. S5(b) has an excitation maximum at 653 nm and an emission maximum at 669 nm. The excitation and emission spectra of the dyes form the basis for selection of excitation lasers in confocal microscopy.

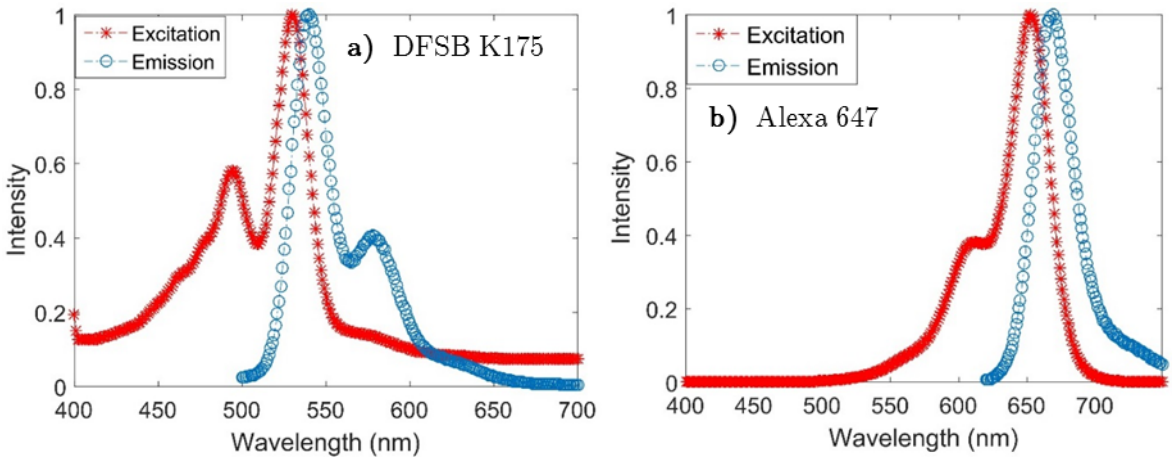

Figure S5: Excitation and emission spectra : a) DFSB K175, and b) Alexa 647.

S4. Confocal microscopy and Image analysis procedure

We use Nikon A1 line scanning confocal microscope for imaging soft striped superhydrophobic surfaces and drop. The lasers used have a wavelength of 488 nm and 638 nm. The emission is collected using a band filter in the range 500 nm to 550 nm for DFSB K175 (soft-structures) and 663 nm to 738 nm for Alexa 647 (drop). Fig. S6 shows the emission collection region for DFSB-K175 and Alexa 647.

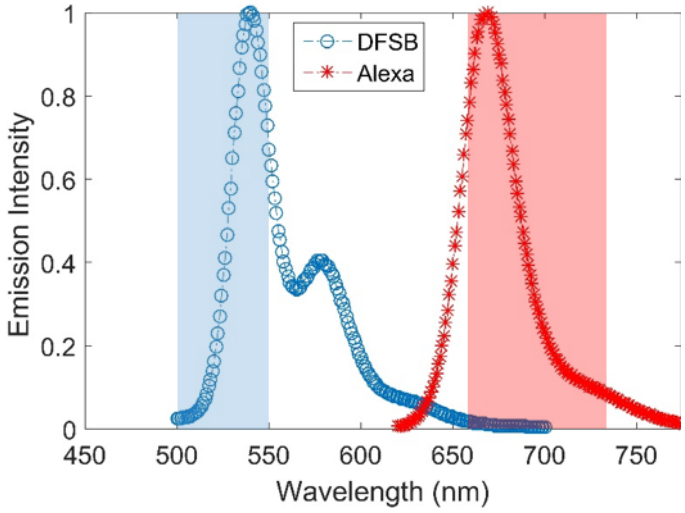

Figure S6: Emission spectra of DFSB-K175 and Alexa 647 with shaded collection region. Blue region spans from 500 nm to 550 nm and red region span from 663 nm to 738 nm.

The blue shaded region is for DFSB-K175 and red region is for Alexa 647. The emission collection regions for DFSB and Alexa do not overlap. Hence the signal recorded in channels do not interfere. In order to visualize the deflection of soft structured surface, we used water immersion objective with 60X magnification and numerical aperture 1.2. An air objective with 20X magnification, numerical aperture 0.85 is also used to have a wider region under study. The lateral and axial resolution of imaging is 203 nm and 338 nm respectively. A 3D scan with an axial step equals 3 μm is taken with a total scanning depth along z axis as $\approx$75 μm.
The 3D scan using confocal microscope consists of stacks of 2D plane (x-y plane). The size

of these planes are 200 μm $\times$ 26 μm located vertically along z axis at intervals of 3 μm. We use ImageJ to construct it into a continuous 3D image. In these 3D images, the two channels consisting of emission signals from the drop and the substrate are merged. Drop is shown red and structured surface (lamallae) as green. Fig. S7 shows a confocal image of drop on lamellae.

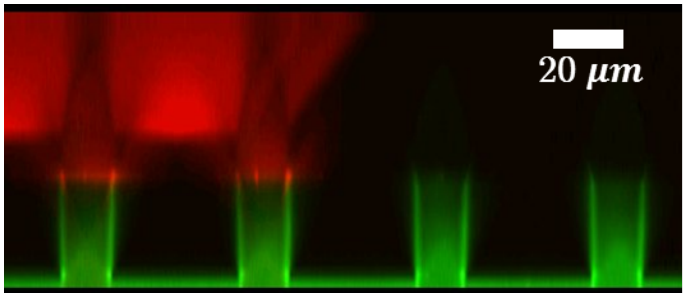

Figure S7: Confocal image of drop on lamallae

The signals from the drop and lamellae are recorded using two seperate channels and in Fig. S7 we see the merged image of two channels. Since there is no significant overlap in the emission spectra of the two dyes (Fig. S6), there is no loss of signal while separating the channels. Thus we get the image of lamellae(x-z slice) for analysis (see Fig. S8(b)). The major steps involved in image analysis are following

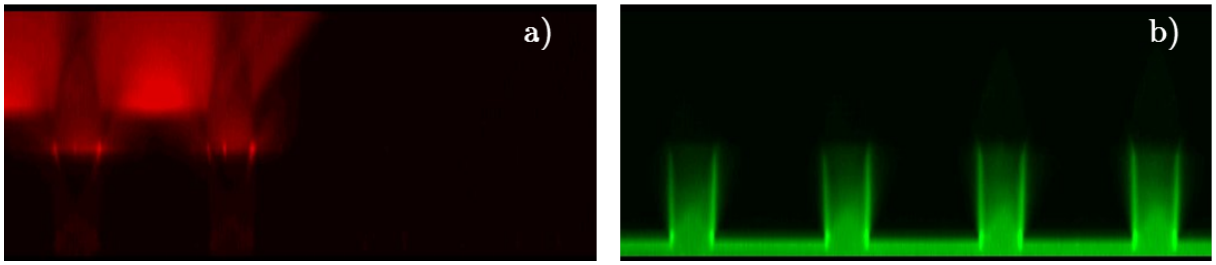

Figure S8: Separated channels. a) Channel 1- Drop, b) Channel 2- substrate

- Edge detection and measurements: We tracked the edges of Fig. S8(b) using homemade Matlab code. Fig. S9 shows the tracked edge using our Matlab routine. The edge detection algorithm includes following steps [6].

  Smoothing of image: The image is smoothened using a Gaussian filter. This step removes the noise from the image.

  Gradients of intensity: This step finds the intensity gradient in x and y direction of any image. The direction of gradient is also calculated as the inverse tangent of the ratio of gradients in two direction.

  Non-Maximal suppression: In the third step each pixel is checked for local maximum condition by comparing the intensity gradient with the neighbouring pixel. If the pixel is not local maximum, it is subjected to zero. If the pixel is local maxima then it is given value 1. This step gives the binary image with edges.

  Double thresholding: In this step, two thresholds are defined. The upper threshold of intensity gradient is decided and the lower threshold is 0.25 times the higher threshold. Any pixel which is above the higher threshold is an edge, any pixel below the lower

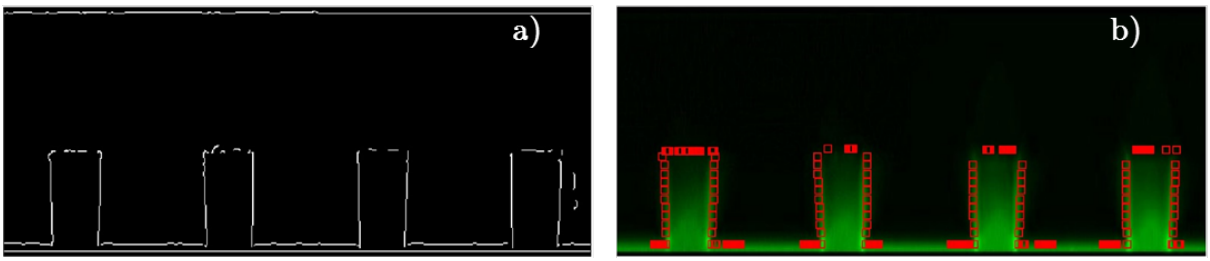

Figure S9: Tracked edges of structures. a) Edges Image of structure after edge detection algorithm, b) Overlap of edges on substrate image. Red points denote the tracked edges and structures are green.

threshold is not an edge. Any pixel between the two threshold is checked for its connectivity with the edges above the higher threshold. If the pixel between the thresholds is connected to pixel above the higher threshold, then this pixel is also defined as edge(Fig. S9 a). Fig. S9 b) shows overlap of detected edge (square Red markers) on the confocal image Fig. S8 b).

In the measurement part we track the left edge of the lamella and inorder to accurately measure the deformed shape , we carefully subtract the initial shape profile of lamella from the deformed profile.

S5. Spreading of the droplet with increasing magnitude of the applied electrical voltage (represented by the electrowetting number η)

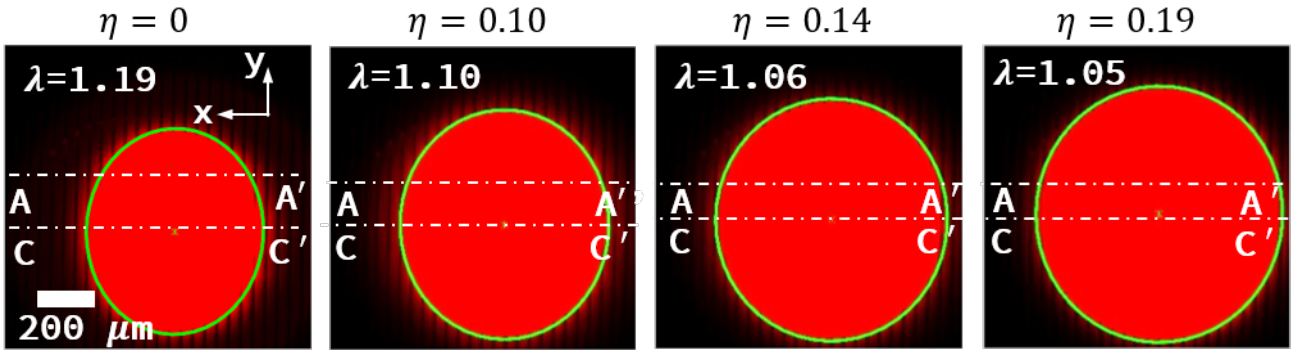

Figure S10: Spreading of drop (red) . AA' is plane where the droplet contact line covers only one top edge of lamella and CC' is plane where the droplet contact line locally covers both the top edge of the lamella. The aspect ratio (α) and Young's modulus (E) of the lamellae are 3.0 and 2.1 MPa respectively. λ denotes the ratio of major to minor axis of the fitted ellipse to the bottom view of drop (green outline to the drop).

At $\eta = 0$, the droplet footprint is elliptical in shape with ratio of length of major axis to minor axis, $\lambda = 1.19$. With increase in electrowetting number (η), the drop spreads across the stripes and its footprint gradually changes from elliptical to circular with $\lambda = 1.05$ for $\eta = 0.19$. For a droplet in Cassie state, the droplet footprint transforms from elliptical to circular shape on the application of electrical voltage in order to minimise the total free energy of the system, which for the present case ideally comprises of the surface energy, the electrostatic energy (see

ref 28) and the elastic energy due to the underlying deformation of the lamellae. An estimate for the total free energy, per unit length, of the system can be written as Eq. (1)

$$E_T \sim (\gamma \tan\frac{\phi}{2} + \frac{\gamma_{sl}^{eff} - \gamma_{sv}}{2})l_c - \frac{1}{2}c_d U_{rms}^2 2\pi\frac{A}{l_c} + E_{el} \tag{1}$$

where γ is the liquid-vapour surface tension, ϕ is the macroscopic contact angle, and γ_{sv} and γ_{sl}^{eff} are the solid-vapour and effective solid-liquid surface tension respectively. c_d is the effective capacitance per unit area of the conductive droplet-substrate system, U_{rms} is the applied AC root mean squared voltage, A is the area of droplet-substrate interface, and l_c is the length of circumference of the droplet footprint. Here, E_{el} is the elastic energy per unit length due to the bending of the lamellae at the droplet contact line. Since the length scale for the bending of a lamella (order of few microns) is very small compared to the droplet length scale (order of a millimeter), E_{el} can be neglected for evaluating the macroscopic shape of the droplet. The important thing to note here is that the contribution of electrostatic energy is negative whereas the surface energy contribution is a positive term in the total energy formulation. Hence, to minimize the total energy under considerably strong EW actuation, the droplet takes a shape with highest A and corresponding minimum l_c. The shape with largest $\frac{A}{l_c}$ is a circle. It must be noted here that this is a qualitative explanation; an exact quantitative prediction of the droplet shape is not trivial because of the anisotropy in the substrate and is beyond the scope of the present work.

S6. Increasing deflection of the lamella at the droplet contact line with decreasing E for $\alpha = 1.3$

In Fig. S11, the left and right coloumns show the lamellae configurations for $\eta = 0$ and $\eta = 0.16$ respectively for decreasing E (different rows). All the lamellae configurations in Fig. S11 are at A-A$'$ with aspect ratio $\alpha = 1.3$. The deformation of the outermost lamella (i.e lamella 2 for $\eta = 0$ and lamella 5 for $\eta = 0.18$) increases with decreasing value of E (Fig. S11). These observations are qualitatively similar to those for higher aspect ratio lamallae (see main text Fig. 4).

S7. Theoretical equilibrium shape of lamella- Elastica Approach

Fig. S12 a) shows the SEM image of the lamallae and capillary forces acting on the lamella top. Fig. S12 b) shows the schematic of deformed lamella with the capillary forces for the mathematical treatment. The relation of the curvilinear coordinate θ and s with the cartesian coordinate x and z is given by,

$$x = \int_0^L \sin\theta ds \tag{2a}$$

$$z = \int_0^L \cos\theta ds \tag{2b}$$

The deformed shape $\delta(z)$ of a soft lamella due to capillary forces can be theoretically determined using variational principle as classically done for problems in linear elasticity. The governing equation is given by Eq. 3 [7]

$$B\theta'' + F_x\cos\theta - F_z\sin\theta = 0 \tag{3}$$

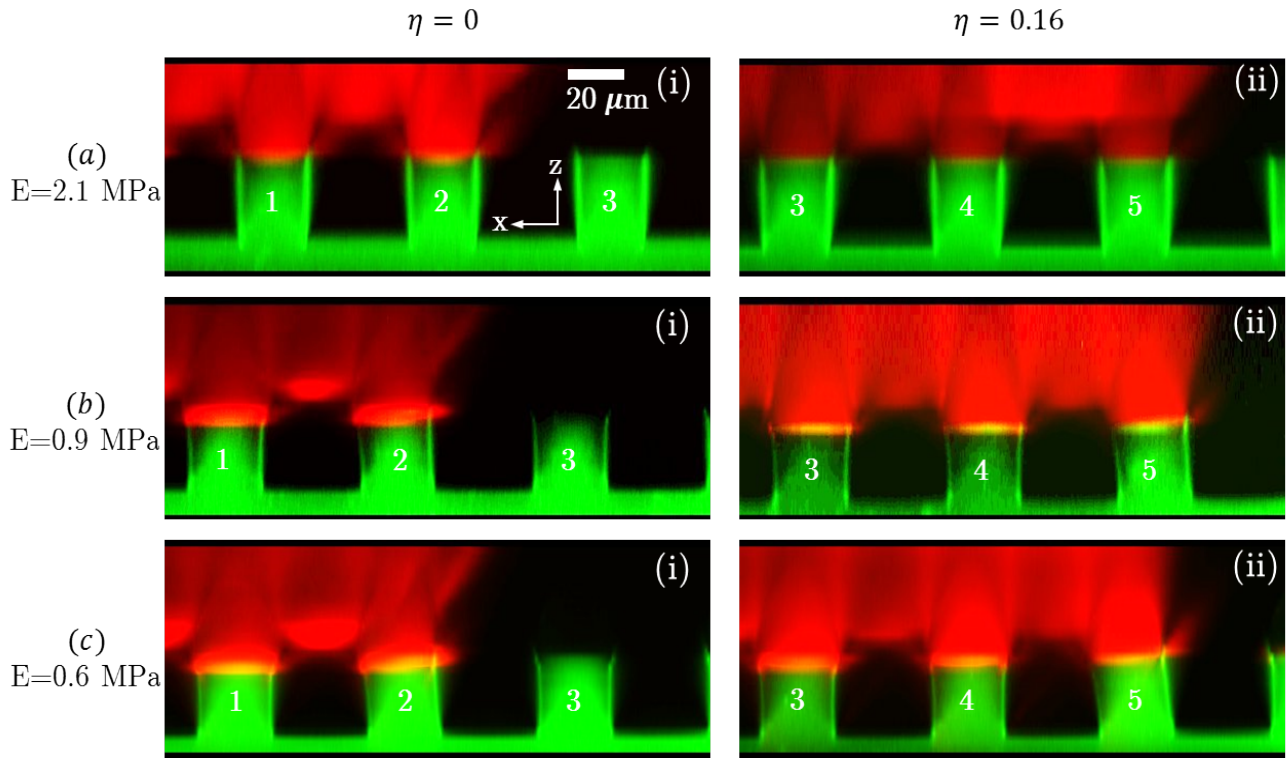

Figure S11: Deflection of lamellae for $\alpha \approx 1.3$ and $\eta = 0, \eta = 0.16$. E varies as 2.1 MPa , 0.9 MPa , 0.6 MPa. The contact line is pinned on lamella 2 and lamella 5 for $\eta = 0$ and $\eta = 0.16$ respectively.

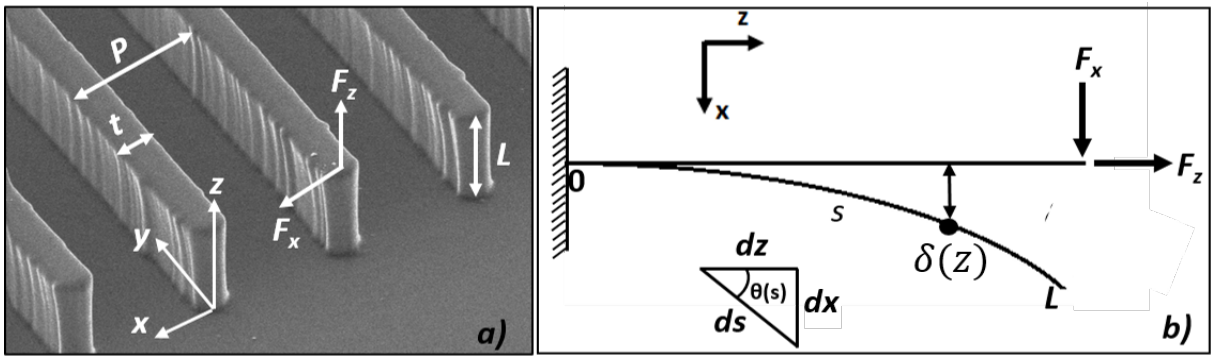

Figure S12: Schematic of lamella subjected to forces. F_x and F_z are forces acting in positive x and positive z direction respectively. s and θ are curvilinear coordinates. $\delta(z)$ is the local deflection of the lamella from the undeformed shape. The small triangle shows the elemental section of the lamella.

where $B = EI/(1-\nu^2)$ is the flexural rigidy for planar structures [8], I is the moment of intertia about the bending axis (here y axis) and $\nu = 0.5$ is the Poisson's ratio [9, 10], F_x and F_z are net horizontal and vertical forces acting on the lamella. The net force on the lamella depends on the angles ψ and ϕ (see main text Eq. 1a to Eq. 1e). These angles are estimated from experimental confocal images and are presented for various cases in Table 1
Furthermore, Eq. 3, along with the boundary conditions,

$$s = 0; \theta = 0 \tag{3a}$$
$$s = L; \theta' = 0 \tag{3b}$$

forms a boundary value problem. We convert this boundary value problem to the initial value problem by reducing the second order differential equation (Eq. 3) into two first order coupled differential equations. We integrate the coupled differential equations as initial value problem, using the ode45 routine of Matlab, which uses Runge-Kutta 4th/5th order integration scheme. To satisfy the boundary condition, we employed shooting technique in which at s=0, we guessed the value of θ' and the solution of θ' at s=L is compared with Eqn. 3b. The initial guess ($\theta'(0)$) is improved untill Eqn. 3b is satisfied.

S8. Effect of electrowetting on deflection of lamella (Theoretical shape from Elastica Approach)

Fig. S13 shows theoretical shapes of deformed lamella at the cross sectional plane A-A′ for increasing value of ψ. It is very clear that the deformation of lamella decreases with increasing value of ψ (compare different lamella prrofiles and their associated ψ). Hence it can be concluded that, if the drop stays in Cassie state, with increasing electrical voltage the deformation decreases.

Table 1: Details of various cases and associated angles ψ and ϕ

At A-A′					
Case	η	α	E(MPa)	ψ	ϕ
1	0	3.0	2.1	110°	-
2	0.19	3.0	2.1	120°	-
3	0	2.2	2.1	110°	-
4	0.18	2.2	2.1	120°	-
5	0	2.2	0.9	110°	-
6	0.18	2.2	0.9	120°	-
7	0	2.2	0.6	110°	-
8	0.18	2.2	0.6	120°	-
At C-C′					
9	0	2.2	0.6	110°	135°
10	0.18	2.2	0.6	125°	130°

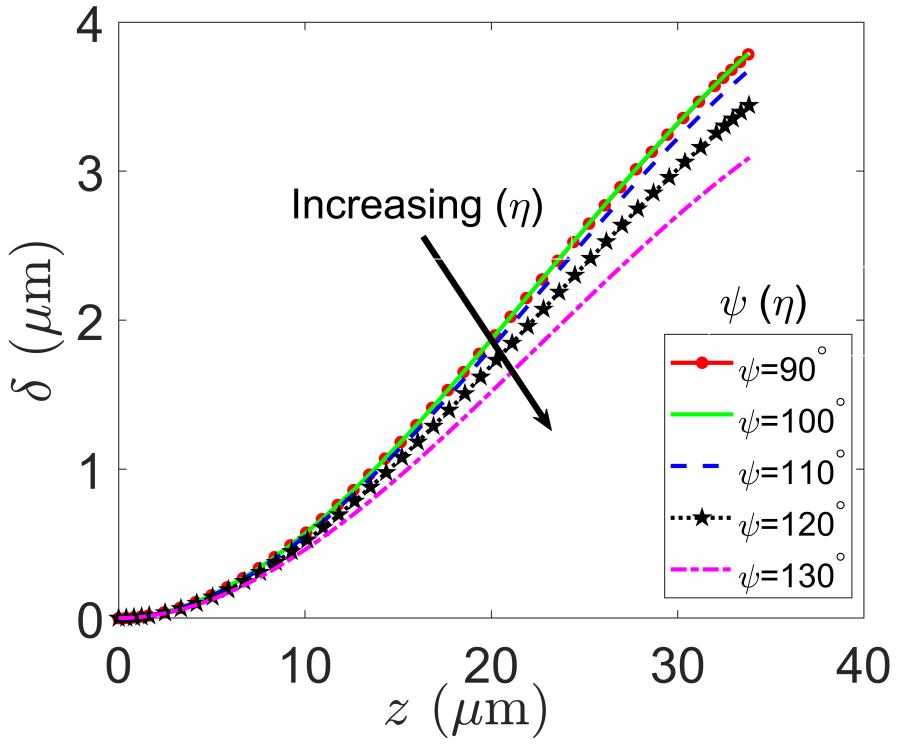

Figure S13: Theoretical deflection profile with increase in η at A-A′. ψ is the angle made be air liquid interface between the lamellae with the vertical. Change in ψ is mediated by change in η. The change in ψ leads to change in capillary forces. The value of E for the plots is 2.1 MPa and α=3.0. Deflection decreases with increasing η.

References

[1] I. D. Johnston, D. K. McCluskey, C. K. L. Tan, and M. C. Tracey, "Mechanical characterization of bulk sylgard 184 for microfluidics and microengineering," *Journal of Micromechanics and Microengineering*, vol. 24, no. 3, p. 035017, 2014. [Online]. Available:

http://stacks.iop.org/0960-1317/24/i=3/a=035017

[2] O. du Roure, A. Saez, A. Buguin, R. H. Austin, P. Chavrier, P. Siberzan, and B. Ladoux, "Force mapping in epithelial cell migration," *Proceedings of the National Academy of Sciences*, vol. 102, no. 7, pp. 2390–2395, 2005. [Online]. Available: http://www.pnas.org/content/102/7/2390

[3] Y.-C. Chuang, C.-K. Chu, S.-Y. Lin, and L.-J. Chen, "Evaporation of water droplets on soft patterned surfaces," *Soft Matter*, vol. 10, pp. 3394–3403, 2014. [Online]. Available: http://dx.doi.org/10.1039/C3SM52719K

[4] Z. Wang, A. A. Volinsky, and N. D. Gallant, "Crosslinking effect on polydimethylsiloxane elastic modulus measured by custom-built compression instrument," *Journal of Applied Polymer Science*, vol. 131, no. 22. [Online]. Available: https://onlinelibrary.wiley.com/doi/abs/10.1002/app.41050

[5] C. Spectraviewer. [Online]. Available: https://www.chroma.com/spectra-viewer

[6] J. Canny, "A computational approach to edge detection," *IEEE Trans. Pattern Anal. Mach. Intell.*, vol. 8, no. 6, pp. 679–698, Jun. 1986. [Online]. Available: https://doi.org/10.1109/TPAMI.1986.4767851

[7] B. Audoly and Y. Pomeau, *Elasticity and geometry: from hair curls to the non-linear response of shells*. Oxford: Oxford University Press, 2010.

[8] L. D. Landau, L. P. Pitaevskii, A. M. Kosevich, and E. M. Lifshitz, *Theory of Elasticity*, 3rd ed. Butterworth-Heinemann, Dec 2012. [Online]. Available: https://www.123library.org

[9] J. O. Iroh and J. Mark, *Polymer data handbook*. Oxford University Press, New York, 1999.

[10] D. W. Inglis, "A method for reducing pressure-induced deformation in silicone microfluidics," *Biomicrofluidics*, vol. 4, no. 2, p. 026504, 2010. [Online]. Available: https://doi.org/10.1063/1.3431715